Macromolecular Research, Vol. 17, No. 10, pp 797-806 (2009)

Mechanical and Thermal Behavior of Polyamide-6/Clay Nanocomposite Using Continuum-based Micromechanical Modeling

Jong-Il Weon*

Reliability Assessment Center of Chemical Materials, Korea Research Institute of Chemical Technology, Daejeon 305-600, Korea

Received February 16, 2009; Revised April 13, 2009; Accepted April 15, 2009

Abstract: The mechanical and thermal behaviors of polyamide-6/clay nanocomposites were studied using the continuum-based, micromechanical models such as Mori-Tanaka, Halpin-Tsai and shear lag. Mechanic-based model prediction provides a better understanding regarding the dependence of the nanocomposites' reinforcement efficiency on conventional filler structural parameters such as filler aspect ratio (α), filler orientation (S), filler weight fraction (ψ_f), and filler/matrix stiffness ratio (E_f/E_m). For an intercalated and exfoliated nanocomposite, an effective, filler-based, micromechanical model that includes effective filler structural parameters, the number of platelets per stack (n) and the silicate inter-layer spacing (d_{001}), is proposed to describe the mesoscopic intercalated filler and the nanoscopic exfoliated filler. The proposed model nicely captures the experimental modulus behaviors for both intercalated and exfoliated nanocomposites. In addition, the model prediction of the heat distortion temperature is examined for nanocomposites with different filler aspect ratio. The predicted heat distortion temperature appears to be reasonable compared to the heat distortion temperature obtained by experimental tests. Based on both the experimental results and model prediction, the reinforcement efficiency and heat resistance of the polyamide-6/clay nanocomposites definitely depend on both conventional (α, S, ψ_f, E_f/E_m) and effective (n, d_{001}) filler structural parameters.

Keywords: micromechanical model, heat distortion temperature, polyamide-6/clay nanocomposite, filler structural parameters.

Introduction

Polymeric materials have been reinforced by inorganic nanofillers, termed polymer nanocomposites, to improve physical and mechanical properties.[1-5] Owing to their remarkable property enhancement, low cost and good processability, polymer nanocomposites are of particular interest. One of the most successful systems has been polymer-layered silicate nanocomposite consisting of organic polymer and inorganic montmorillonite. Polymer-layered silicate nanocomposites are of interest because of their exceptional reinforcement effects at very low filler loading, compared with what is typically required with conventional fillers. This characteristic can be exploited to help design a more customized composite structure because lower nanofiller loading results in lighter structural components. Furthermore, only marginal losses in toughness and ductility are observed in such nanocomposite systems.[1]

Polyamide-6/clay nanocomposites have shown improvements in a variety of physical and thermal properties, such as modulus, strength, thermal stability, gas barrier properties, etc. Furthermore, such significant property enhancements are obtainable at very low nanoclay content. Shepherd *et al.*[6] proposed that single clay layer could be one of ideal reinforcing nanofillers in 1974, due to their extremely high aspect ratio and the nanometer filler thickness. Clay layers have high cation exchange capacity (CEC), which allows surface modification of the clay interlayer to achieve better compatibility with a host polymer matrix. In addition to high CEC, clay is an abundant, inexpensive inorganic material. Those advantages have let to large-scale commercial uses. Moreover, an outstanding research by the Toyota group[7-9] has drawn forth efforts of many researchers on polymer-clay nanocomposites.

Nanoclay has plate-like structures that have large surface areas and high aspect ratio. Thus, the reinforcement efficiency on the physical and mechanical properties strongly depends on the filler structural parameters such as filler shape, filler aspect ratio, filler modulus, filler volume fraction, interfacial adhesion, surface characteristics and filler orientation.[1,10-12] The literatures dealt with the effect of filler structural parameters of nanocomposites on their mechanical properties are nearly rare. A few of recent studies[13,14] tried to examine how the nanofiller structural parameters (e.g., shape, aspect

*Corresponding Author. E-mail: jiweon@krict.re.kr

ratio and orientation) affect the mechanical properties using micromechanics-based composite models. These specific models not only involve a number of assumptions[13] that are inadequate for describing the actual nanocomposite characteristics but also can not exactly address the morphology in terms of the effect of filler structural parameters. Although the micromechanics-based models cannot completely describe the mechanical and thermal behaviors of nanocomposite systems, there have still been good correlations with experimental results.

Particular attention of this paper is to gain a better understanding on the reinforcement efficiency and heat resistance of polyamide-6/clay nanocomposites using continuum-based micromechanical model. Both the Halpin-Tsai and Mori-Tanaka models are exploited to account for the reinforcement efficiency and heat resistance of nanocomposites depending on the nanofiller structural parameters. The effective filler-based micromechanical model, which includes effective clay structural parameters, the number of platelet per stack (n) and the silicate inter-layer spacing (d_{001}), is proposed. The potentiality for predicting macroscopic mechanical and thermal properties of nanocomposites regarding various structural parameters of nanofiller is examined. Based on this micromechanical model, the fundamental structure-property relationship of polymer nanocomposites is widely addressed.

Experimental

Materials. Commercially available pellets of neat polyamide-6 (grade #: 1022B) and 2 wt% layered silicate-based polyamide-6 nanocomposite (grade #: 1022C2) were obtained from Ube Industries, Ltd., Japan. First of all, the pellet was dried at 100 °C for 12 h in vacuum oven and then was extruded using a HaakeBuchler Rheocord (system 40) at a rotational speed of 30 rpm. The temperature profiles of the barrel were set at 235-245-255-260 °C toward the inlet of injection mold and the mold temperature was set at 180 °C. After molding, the samples were quenched in water and air-dried. The resulting plates were immediately sealed in a polyethylene bag and kept in a vacuum desiccator to avoid moisture absorption. In addition, a simple shear process was performed to alter the aspect ratios and orientation of the clay nanoparticles. This process was carried out at 60 °C and with a rate of 0.25 mm/s using a servo-hydraulic mechanical system (MTS-810). The processed samples were labeled as follows: Reference-received no processing, A1-received a single pass and C2-received two processing pass with a 180° rotation of specimen between the passes. A detailed description of simple shear process is available in Refs..[1,15-17] All samples were annealed at 150 °C for 3 h. The annealing process has been well known to be a useful technique for relaxing molecular orientation and pre-existing morphology in the matrix due to processing. Furthermore, the heating chamber was purged with nitrogen gas to minimize sample oxidation during annealing.

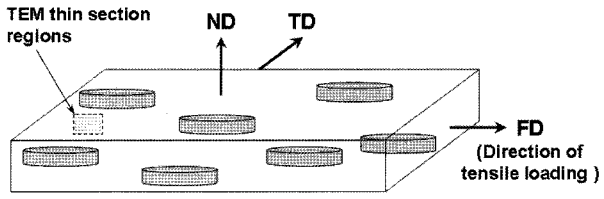

Figure 1. Schematic of samples used for mechanical test and TEM observation; note that ND: normal direction, TD: transverse direction and FD: flow direction.

Microscopy and Image Analysis. For transmission electron microscopy (TEM) observation, ultra-thin sections of 60 to 80 nm in thickness were prepared under cryogenic environment using a Reichert-Jung Ultracut E microtome with a diamond knife. The thin sections were placed on the 100-mesh Formvar/carbon-coated copper grids and examined using a JEOL JEM-2010A transmission electron microscope operating at an accelerating voltage of 200 kV. Samples for TEM analysis were cut parallel to the flow direction (FD), as depicted in Figure 1. A semi-automated image analysis procedure[18] was performed on TEM micrographs to quantify the clay aspect ratio and degree of clay orientation of the polyamine-6/clay nanocomposites.

Tensile Test. The tensile specimens parallel to the flow direction were tested using a screw-driven mechanical testing machine (Sintech II) at a constant crosshead speed of 0.085 mm/s. An extensometer was employed to measure the displacement in the gauge length region. Young's modulus was calculated at 1% strain in accordance with the ASTM D638 standard. The average value and standard deviation were recorded after testing five specimens of each sample.

Dynamic Mechanical Analysis. The dynamic mechanical analysis (DMA) spectra were evaluated under torsional mode on a Rheometric Mechanical Spectrometer (RMS-800) at temperatures ranging from -140 to 250 °C. The DMA specimens were cut parallel to the flow direction. Measurements were set at 5 °C intervals with 45 s of soaking time. The spectrometer was set to produce a sinusoidal wave function with a peak strain of 0.1% and frequency of 1 Hz.

Heat Distortion Temperature Test. Heat distortion temperature (HDT), one of key factors that can address load-bearing ability at elevated temperature, was measured according

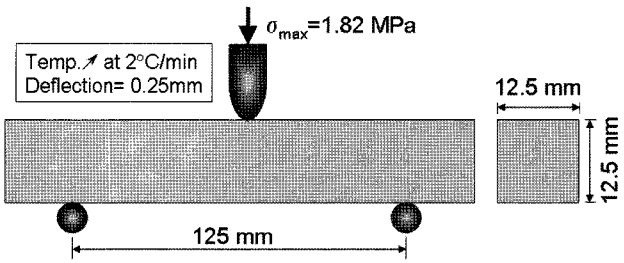

Figure 2. Schematic diagram of heat distortion temperature testing.

to ASTM D 648. The HDT specimens parallel to the flow direction were tested using a Ceast HDT vicat auto apparatus at a heating rate of 2 °C/min and a load of 1.82 MPa. Figure 2 shows the schematic diagram for HDT measurement. For each sample, the HDT value reported was the average of at least three tests.

Continuum-based Micromechanical Models

Conventional Filler-based Micromechanical Model. Numbers of mechanic-based models have provided a reasonable prediction for the properties of filler-based composite materials. Especially, the reinforcement efficiency mechanisms have been presented using those theoretical and numerical models.[19-29] In conventional micromechanical models, the effect of filler volume fraction (ϕ_f), filler aspect ratio (α), filler orientation (S) and filler modulus (E_f) or filler/matrix stiffness ratio (E_f/E_m) are explored as important factors for predicting the macroscopic composite properties.

It is well known that Halpin-Tsai and Mori-Tanaka theories are wildly applied to predict the stiffness of discontinuous fiber-reinforced composites. Mori-Tanaka theory[20] offered the best prediction for the properties of composites with relatively large aspect ratio of fillers. The models based on Halpin-Tsai theory[21-23] provided reasonable estimations for reinforcement efficiency of composite materials. Figure 3 shows the three principle orthogonal directions used to calculate composite stiffness corresponding (a) Halpin-Tsai and (b) Mori-Tanaka models. The longitudinal engineering stiffness (E_{11}) and the transverse engineering stiffness (E_{33}) of the Halpin-Tsai and the Mori-Tanaka models are expressed in eqs. (1) and (2), respectively.

$$\frac{E_{11}}{E_m} = \frac{1+2(l/t_f)\eta\phi_f}{1-\eta\phi_f} \qquad (1a)$$

$$\frac{E_{33}}{E_m} = \frac{1+2\eta\phi_f}{1-\eta\phi_f}$$

$$\eta = \frac{E_f/E_m - 1}{E_f/E_m + 2(l/t_f)} \qquad (1b)$$

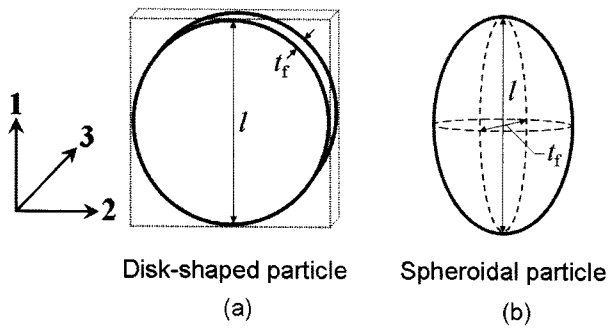

Figure 3. Three principle orthogonal directions used to calculate nanocomposite modulus corresponding; (a) Halpin-Tsai and (b) Mori-Tanaka models.

where l is the filler length and t_f is the filler thickness.

$$\frac{E_{11}}{E_m} = \frac{1}{1+\phi_f[-2\nu_m A_3 + (1-\nu_m)A_4 + (1+\nu_m)A_5 A]/2A} \qquad (2a)$$

$$\frac{E_{33}}{E_m} = \frac{1}{1+\phi_f(A_1 + 2\nu_m A_2)/A} \qquad (2b)$$

where ϕ_f is the filler volume fraction, ν_m is the Poisson ratio of the matrix, A, A_1, A_2, A_3, A_4 and A_5 are calculated from the matrix, filler properties and components of the Eshelby tensor,[19] which depend on the filler aspect ratio (l/t_f) (where l and t_f are the major and minor diameters of an ellipsoidal disk-shaped inclusion) and dimensionless elastic constants of the matrix. Complete details of these variables are given in ref..[26]

The filler orientation in a polymer matrix has a significant effect on composite stiffness. Completely unidirectional alignment of fillers in a polymer matrix can rarely be achieved due to fillers' structural characteristics and processing difficulties. Disk-shaped fillers have the same reinforcement efficiency in orthogonal direction, E_{11} and E_{22} (Figure 3). In order to estimate the modulus enhancement of composites with randomly oriented filler, the following equation may be used:[30,31]

$$E_{radom-3D}^{platelet} = 0.49E_{11} + 0.51E_{33} \qquad (3)$$

Shear Lag Model. In particular, rigid particles are naturally resistant to relatively high stress or strain. When such particle-filled composites are subject to axial load, a significant portion of the load is transmitted from the surrounding matrix to the rigid particles through shear stress at the interface. Shear lag model[29] is employed to address the load-transfer efficiency on α, E_f/E_m.

$$\sigma_f = E_f\varepsilon\left[1 - \left(\frac{\cosh\left(\frac{2x\lambda\alpha}{l}\right)}{\cosh(\lambda\alpha)}\right)\right] \qquad (4a)$$

$$\tau_i = \frac{\lambda E_f \varepsilon}{2}\left[\frac{\sinh\left(\frac{2x\lambda\alpha}{l}\right)}{\cosh(\lambda\alpha)}\right] \qquad (4b)$$

$$\lambda = \left[\frac{4G_m}{E_f \ln(\phi_f)}\right]^{1/2}$$

where ε is the applied strain, x is the distance from the center of filler, τ_i is the interfacial shear stress along the filler length, and G_m is the shear modulus of the matrix.

The shear lag model appears that large aspect ratio (α) and high E_f dominantly enable fillers to bear a large portion of the applied load.

Results and Discussion

Microscopy Investigation. Figure 4 shows the TEM micrographs that indicate different clay aspect ratio and orientation of the simple-shear-processed and then annealed nanocomposites. Reference polyamine-6/clay nanocomposite, which received no simple shear deformation, shows well-exfoliated clay structure along the flow direction (Figure 4(a)). Also, it is observed that clay lengths and orientations of the A1 and C2 polyamide-6/clay nanocomposites have been varied upon the simple shear process (Figure 4(b) and 4(c)). A semi-automated image analysis scheme was performed to quantify these variations. It should be mentioned that three different TEM micrographs from each sample were used to enhance the reliability of the image analysis. The aspect ratios (α) of dispersed platelets are calculated by:

$$\alpha = \frac{\bar{l}}{\bar{t}} \tag{5}$$

where $\bar{l}$ is mean platelet length and $\bar{t}$ is mean platelet thickness (= 0.94 nm[13]).

The degree of platelet orientation (S) of can be defined as (i.e., standard deviation):

$$S = \sqrt{\frac{\sum_{i=1}^{n}(\Phi_i - \bar{\Phi})^2}{N}} \tag{6}$$

where Φ_i is the actual platelet orientation, $\bar{\Phi}$ is the mean platelet orientation and N is total number of platelets counted. Note that the degree of platelet orientation was determined in relation to the uniaxial loading condition on which tensile test was performed.

Table I. The Results of TEM Image Analysis for the Reference, A1 and C2 Polyamide-6/Clay Nanocomposites

Sample	Aspect Ratio (α)	Degree of Orientation* (S)
NC_Ref.	132±33	12°
NC_A1	87±26	10°
NC_C2	78±21	24°

*Degree of platelet orientation from unidirectional reinforcement.

Table I summarizes the results of image analyses. A careful observation reveals that the A1 process only reduces the clay aspect ratio, while the C2 route alters both the clay aspect ratio and the clay orientation. Those results will be applied to the predictions of mechanical and thermal property for polyamide-6/clay nanocomposites using the micromechanical models.

Tensile Property. The key tensile properties with dependence on clay aspect ratio and orientation are reported in Table II. A drop in aspect ratio from 132 to 87 results in a large reduction in modulus. In addition, the degree of clay orientation from unidirectional reinforcement has an effect on modulus. The C2 nanocomposite, which has a more randomly dispersed clay and lower aspect ratio, reveals a decrease of ~19% in modulus compared to that of the reference nanocomposite.

Dynamic Mechanical Analysis. The dynamic mechanical properties (e.g., the storage modulus as a function of temperature) for the nanocomposites are shown in Figure 5(a). The reinforcing effect is observed depending on the clay aspect ratio and orientation. These results are in good agreement with those of tensile test (Table II). It is clearly found that the reinforcing effect of the nanocomposite systems is highest at

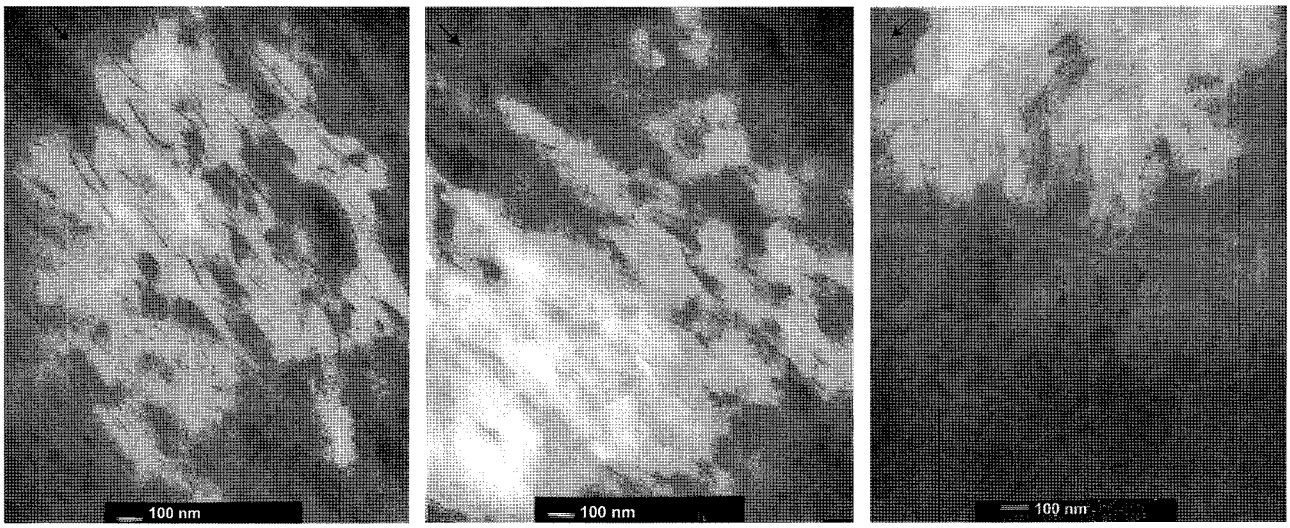

(a) (b) (c)

Figure 4. Typical TEM micrographs of the simple-shear-processed polyamine-6/clay nanocomposites (NC) used for image analysis; (a) NC_Reference, (b) NC_A1 and (c) NC_C2. The arrows indicate the flow direction.

Table II. Mechanical Properties of the Reference, A1 and C2 Polyamide-6/Clay Nanocomposites

Sample	Storage Modulus, G' (Pa)		Young's Modulus (GPa)
	@ 25 °C	@ 100 °C	
NC_Ref.	1.28×10^9	3.33×10^8	4.67±0.20
NC_A1	1.12×10^9	2.89×10^8	4.09±0.18
NC_C2	1.07×10^9	2.51×10^8	3.80±0.14

Standard deviation for the five samples tested.

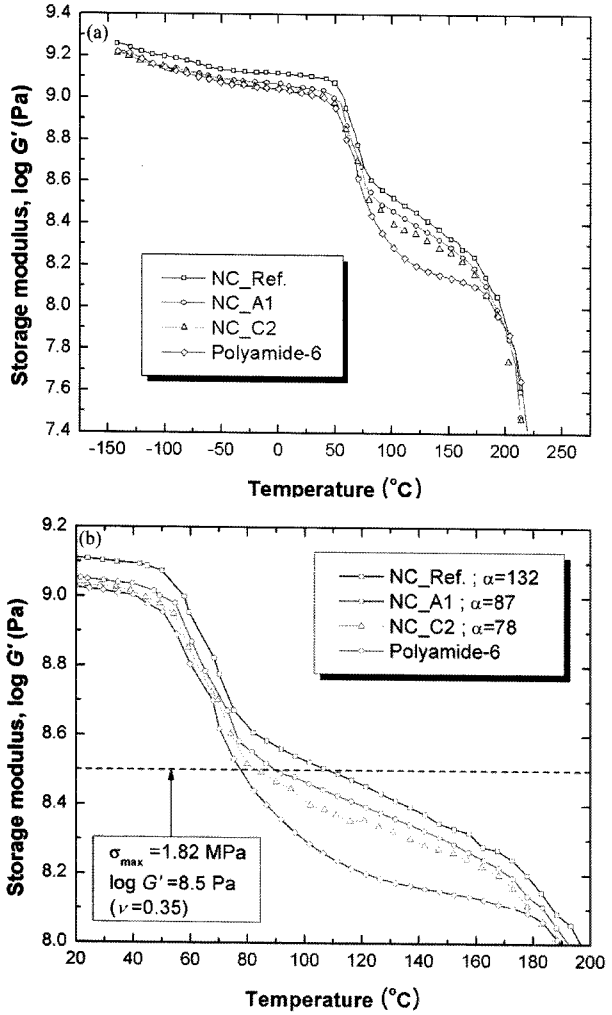

Figure 5. Dynamic mechanical spectra for the neat polyamide and nanocomposites: (a) storage modulus and (b) the HDT determined from the plot of log G' vs. temperature.

temperature between glass transition temperature (T_g) and melting temperature (T_m) compared to that of neat polyamide-6. This may has an effect on the heat resistance of the nanocomposites.

Heat Distortion Temperature Test. The heat distortion temperature (HDT) depending on clay aspect ratio and orientation are summarized in Table III. A decrease in both clay aspect ratio and orientation results in virtual decrease in HDT. A couple of literatures[13,32,33] reported that the HDT of a polymeric material can be estimated from the DMA results. Figure 5(b) illustrates HDT values obtained from storage modulus vs. temperature curve of DMA spectrum. The logarithmic storage modulus (log G') of 8.5 Pa corresponds a stress of 1.82 MPa defined in HDT. The high aspect ratio and reinforcement effect lead to a large increase in HTD, which is excellently consistent with the prior HDT test results.

Table III. Heat Distortion Temperature for the Reference, A1 and C2 Polyamide-6/Clay Nanocomposites

Sample	HDT[a] (°C)	HDT[b] (°C)	HDT[c] (°C)
NC_Ref.	112	110	157
NC_A1	95	90	116
NC_C2	82	84	111

[a]Obtained by experimental HDT test. [b]Determined by experimental DMA test. [c]Predicted by Halpin-Tsai model prediction.

Conventional Filler-Based Model Property.

Effect of (ψ_f, α, E_f/E_m, S) on Nanocomposite Modulus: The effect of filler weight fraction (ψ_f), aspect ratio (α) and filler/matrix stiffness ratio (E_f/E_m) on the longitudinal modulus improvement (E_{11}/E_m) is examined using the Halpin-Tsai (H-T) and Mori-Tanaka[1)] (M-T) theories. The model predictions demonstrate the dependence of E_{11}/E_m on ψ_f, α, E_f/E_m and S (Figures 6-7).[2)] Both models display similar predicted trends. However, the Mori-Tanaka model clearly shows more conservative results than those in the Halpin-Tsai model. This difference may be derived from the assumptions inherent for both models.[1] It should be noticed that the modulus enhancement (E_{11}/E_m) appears to be non-linear as α and E_f/E_m increase (Figure 6(b) and 6(c)). However, the better reinforcement efficiency is still observed at the larger α and the higher E_f/E_m. This nature will be addressed in detail later using shear lag model.

Using the Halpin-Tsai and Mori-Tanaka theories, the influence of filler orientation on reinforcement efficiency of nanocomposite is investigated (Figure 7). It should be mentioned that the radom-3D reinforcement efficiency is higher than that of the transversely oriented composite. Misalignment of unidirectional reinforcement causes significant decrease in modulus.

Figure 8 depicts the dependencies of axial stress in filler and shear stress at interface, normalized to the applied strain (ε=0.1%), on α and E_f/E_m. Interestingly, the larger aspect ratio (α) is, the higher maximum axial and shear stresses as

[1)]The Poisson's ratio of the polyamide-6 and the clay used in the Mori-Tanaka model prediction of the nanocomposites are 0.35 and 0.2,[13,14] respectively.

[2)]For the prediction of conventional filler-based model, the filler modulus (E_f) used is 178 GPa.[13,37]

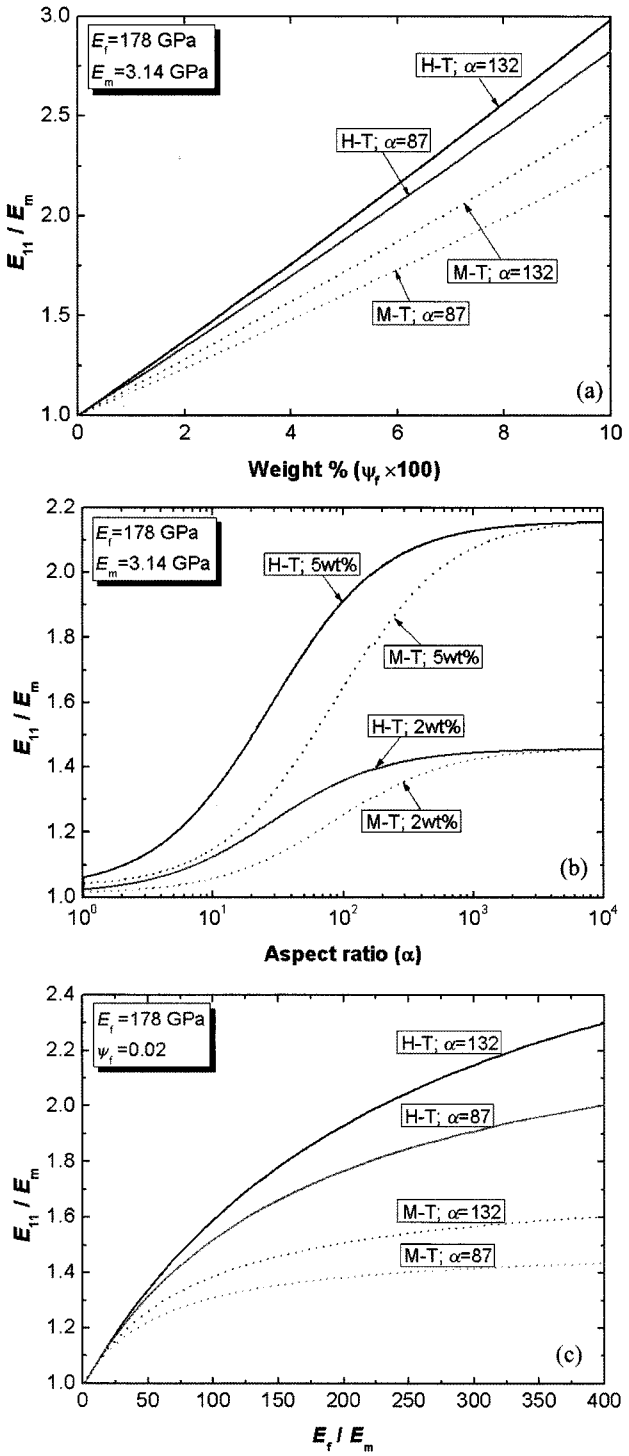

Figure 6. Conventional filler-based model prediction of the Halpin-Tsai (H-T) and the Mori-Tanaka (M-T) theories; (a) effect of filler weight fraction (ψ_f), (b) aspect ratio (α) and (c) filler/matrix stiffness ratio (E_f/E_m) on the longitudinal modulus improvement (E_{11}/E_m).

well as the longer load-carrying filler length have (see Figure 8(a) and 8(b)). At a certain aspect ratio, the maximum axial stress converges to constant value, approaching to the saturation

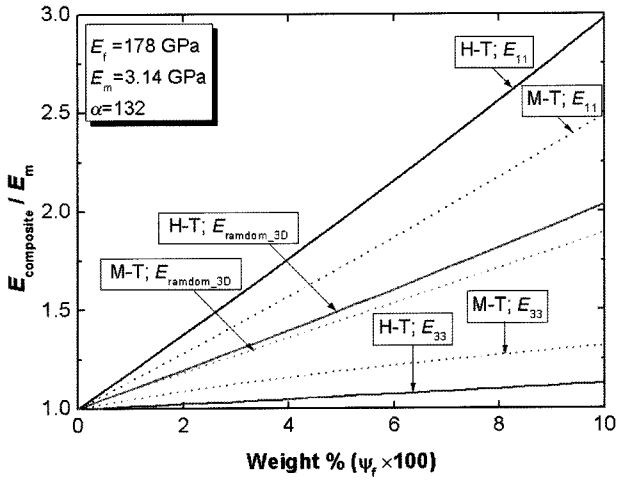

Figure 7. The effect of filler orientation (S) on reinforcement efficiency of nanocomposites as predicted by the Halpin-Tsai (H-T) and the Mori-Tanaka (M-T) theories.

point of E_{11}/E_m as shown in Figure 6(c). The saturation point of E_{11}/E_m at high E_f/E_m is a result of combination of two counter-balancing factors: the high E_f causes to increase in modulus of nanocomposites, but the low G_m/E_f ratio leads to decrease in the load-carrying efficiency. It is observed that decreases in load-carrying filler length with increasing E_f/E_m and G_m/E_f (Figure 8(c)).

It should be mentioned that when aspect ratio is 80 and 130, the maximum axial stress in filler, the maximum shear stress in interface, and the sufficiently load-carrying filler length appear to be satisfied. Therefore, those results may lead to a significant reinforcement efficiency of the nanocomposites shown in tensile results.

Effective Filler-based Model Property.

Effective Filler-based Micromechanical Models: The dispersion of fillers in a polymer matrix is typically described in terms of exfoliation or intercalation. Fully exfoliated nanocomposites are considered to consist of single clay layers dispersed in a polymer matrix, while in the intercalated systems, inter-layer domains of fillers (e.g., clay particles) are penetrated by polymer chains and consequently stacked with an inter-layer spacing of 1-4 nm, typically. However, conventional filler-based micromechanical models for predicting the macroscopic properties of nanocomposites were not considered those nanoclay structural parameters, which regards that nanocomposites just consist of two homogeneous phases, fillers and matrix. In an earlier work by Boyce,[14] in order to explain the geometric natures of intercalated clay they proposed the effective particles, which consist of the clay layers and clay inter-layer galleries. Therefore, effective filler structural parameters, the number of platelet in a stack (n) and the silicate inter-layer spacing (d_{001}), are used to assess macroscopic property enhancement of particle-filled nanocomposites. Mechanics-based models for nanoclay structure are

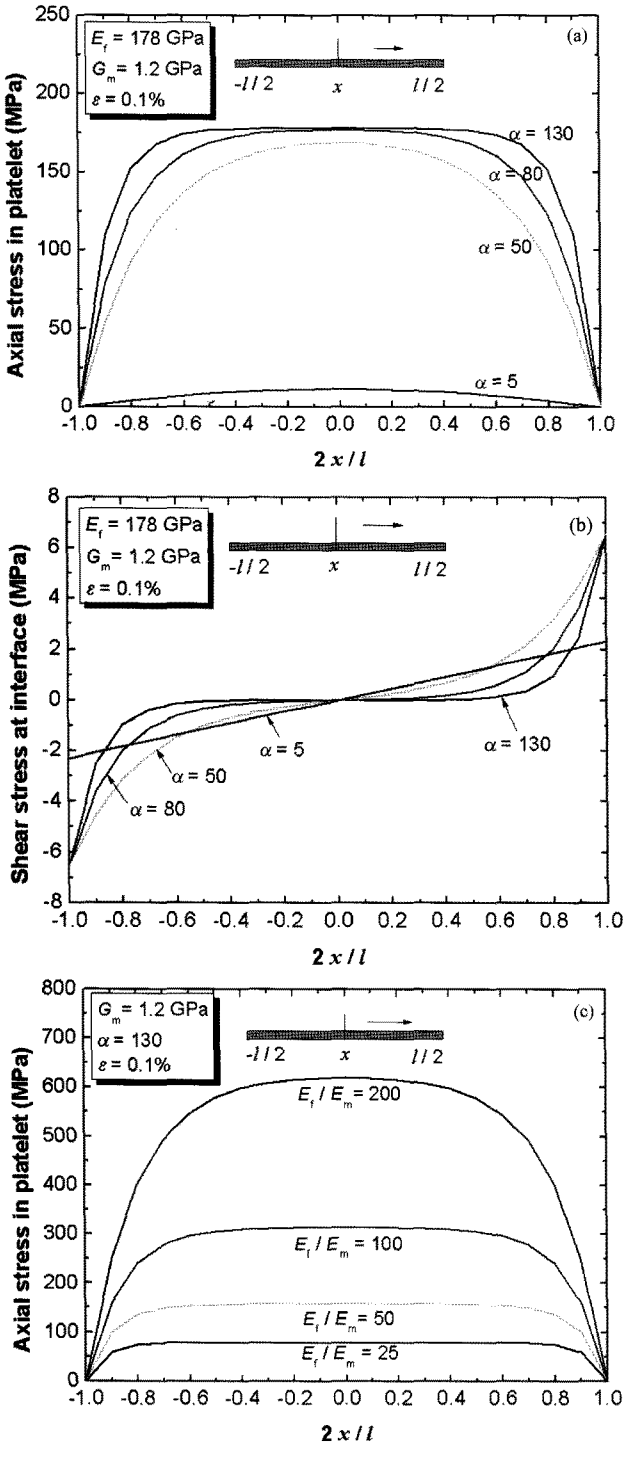

Figure 8. Normalized stress distribution along filler and at interface between filler and matrix; x is the distance along the filler. (a) effect of filler aspect ratio on axial stress, (b) effect of filler aspect ratio on the shear stress and (c) effect of filler modulus on axial stress.

established by mapping of the effective filler structural parameters (n, d_{001}) to the conventional filler structural parameters (α, ϕ_f, E_f/E_m).

The thickness of effective filler (t_f^{eff}) can be expressed in terms of n and d_{001} by the following equation:[13]

$$t_f^{eff} = (n-1)d_{001} + t_{platelet} \tag{7}$$

where $t_{platelet}$ is the thickness of a silicate platelet.

The number of platelets per effective filler thickness (κ):[14]

$$\kappa = \frac{n}{t_f^{eff}} = \frac{n}{(n-1)d_{001} + t_{platelet}} \tag{8}$$

$$\frac{V_{platelet}}{V_f^{eff}} = \frac{nt_{platelet}}{(n-1)d_{001} + t_{platelet}} = \kappa t_{platelet} \tag{9}$$

where $V_{platelet}$ and V_f^{eff} are the volumes of the platelet in a stack and the effective filler, respectively.

Effective filler aspect ratio (α^{eff}) of can be written as:

$$\alpha^{eff} = \frac{l}{t_f^{eff}} = \frac{l}{(n-1)d_{001} + t_{platelet}} \tag{10}$$

For a nanocomposite system, the effective filler weight fraction (ψ_f^{eff}) is not equal to the filler weight fraction (ψ_f) because the filler is composed of two components, i.e., platelet and inter-layer gallery.

$$\frac{\psi_f}{\psi_f^{eff}} = \frac{\rho_f V_f}{\rho_{platelt} V_{platelt}} = \frac{\rho_f}{\rho_{platelt}} \cdot \frac{1}{\kappa} \tag{11}$$

where ρ_f and $\rho_{platelet}$ is the density of filler and platelet, respectively.

Thus, effective filler volume fraction (ϕ_f^{eff}) can be written as a function of the effective filler weight fraction (ψ_f^{eff}).

$$\phi_f^{eff} = \frac{[(n-1)d_{001} + t_{platelet}]}{nt_{platelet}} \cdot \frac{\rho_m}{\rho_f} \cdot \psi_f^{eff} \tag{12}$$

where $\rho_{platelet}$ and ρ_m is 2.83 and 1.14 (g/cm^3),[13] respectively.

$$\psi_f^{eff} = \frac{2.5nt_{platelet}}{(n-1)d_{001} + t_{platelet}} \cdot \phi_f^{eff} \tag{13}$$

For a fully exfoliated nanocomposite (i.e., n=1), $\psi_f^{eff} = 2.5\,\phi_f^{eff}$. The same result has been shown in ref..[34]

If $E_{gallery} \ll E_{platelet}$, the effective filler modulus can be expressed as the following equation;[14]

$$E_f^{eff} = \frac{nt_{platelet}E_{platelet}}{[(n-1)d_{001} + t_{platelet}]} \tag{14}$$

Effect of (n, d_{001}) on Nanocomposite Modulus: The effect of effective filler structural parameters (n, d_{001}) on reinforcement efficiency of nanocomposite is shown in Figure 9. The dependence of filler/matrix stiffness ratio (E_{11}/E_m) on the number of platelet in a stack (n) and the silicate inter-layer spacing (d_{001}) is examined using the Mori-Tanaka model. E_{11}/

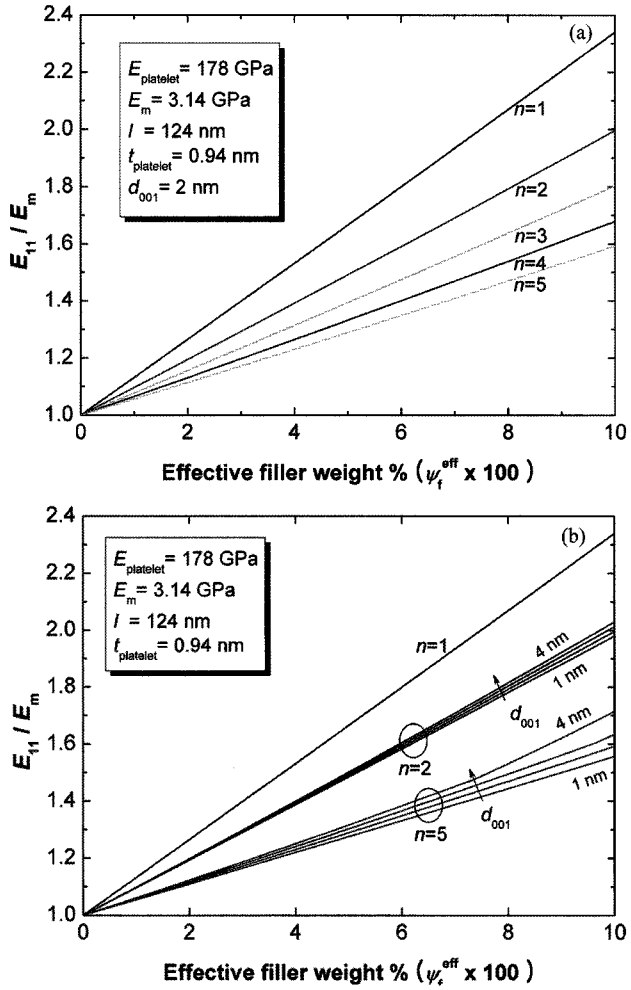

Figure 9. Effective filler-based model prediction of the Mori-Tanaka theories; (a) effect of the number of platelet in a stack (n) and (b) effect of inter-layer spacing (d_{001}) on the longitudinal modulus improvement (E_{11}/E_m).

E_m is plotted as a function of effective weight % (ψ_f^{eff} ×100) and the number of platelet in a stack (n) at a fixed inter-layer spacing (d_{001}=2 nm). Figure 9(a) shows that E_{11}/E_m definitely depend on n. It should be to note that the incremental amount of E_{11}/E_m gradually enlarges as n goes to 1 but a significant increase is not observed even though n goes from 2 to 1, which means that clay layers are exfoliated. Based on the effective filler-based model proposed, an increase in the number of platelet per stack (n) inherently leads to decrease the effective filler aspect ratio (α^{eff}) and modulus (E_f^{eff}) which induce to decrease E_{11}/E_m (see eqs. 10 and 14), but increase the effective filler volume fraction (ϕ_f^{eff}) which induce to increase E_{11}/E_m (see eq. 12). Here, as n decreases, the effect of ϕ_f^{eff} on reinforcement efficiency is suppressed by the effect of α^{eff} and E_f^{eff} (see eqs. 7, 15 and 16). In other words, α^{eff} and E_f^{eff} takes an active role on reinforcement efficiency in case of a fully exfoliated nanocomposite system, while the effect of ϕ_f^{eff} is minimized.

On the other hand, the dependence of filler/matrix stiffness ratio (E_{11}/E_m) on the silicate inter-layer spacing (d_{001}) is plotted as a function of ψ_f^{eff}, n and d_{001} (Figure 9(b)). As d_{001} increase, the incremental amount of E_{11}/E_m increase is smaller compared to the effect of n. It is found that the smaller n is, the smaller increase in E_{11}/E_m is observed. However, in the case of highly intercalated nanocomposite (e.g., d_{001}=4 nm, n=5), a quite strong enhancement in E_{11}/E_m is observed. Oppositely, an increase in d_{001} inherently results in a decrease in E_f^{eff} and α^{eff} which cause to decrease E_{11}/E_m (see eqs. 10 and 14), but an increase in ϕ_f^{eff} which causes to increase E_{11}/E_m (see eq. 12). Here, as d_{001} increases, the effect of ϕ_f^{eff} on reinforcement efficiency is predominant relative to the effect of E_f^{eff} and α^{eff}. i.e., for a highly intercalated nanocomposite system, ϕ_f^{eff} has an strong effect on reinforcement efficiency, while the effect of α^{eff} and E_f^{eff} is minor.

Based on above observations using the effective filler-based micromechanical model, an increase in reinforcement efficiency related to decreasing the number of platelet a stack (n) results from an increase in effective filler aspect ratio (α^{eff})and modulus (E_f^{eff}), while an increase in reinforcement efficiency associated with increasing silicate inter-layer spacing (d_{001}) results from an increase in effective volume fraction (ϕ_f^{eff}). It should be noted that a fully exfoliated nanocomposite (n=1) did not show a significant increase in reinforcement efficiency. In addition, in order to evaluate more exact reinforcement efficiency of nanocomposites using the effective filler-based micromechanical model, the filler orientation (S) should be considered since its effect on modulus improvement is also strong, as shown in Figure 7. In particular, TEM micrographs show that exfoliated clay layer is slightly curved shape (Figure 10). Those curvatures of clay layers may negatively have an effect on reinforcement efficiency of nanocomposites. Therefore, it may not be necessary for an improvement in modulus of nanocomposites to achieve a nearly perfect exfoliation and dispersion of layer-structured nanofiller in a

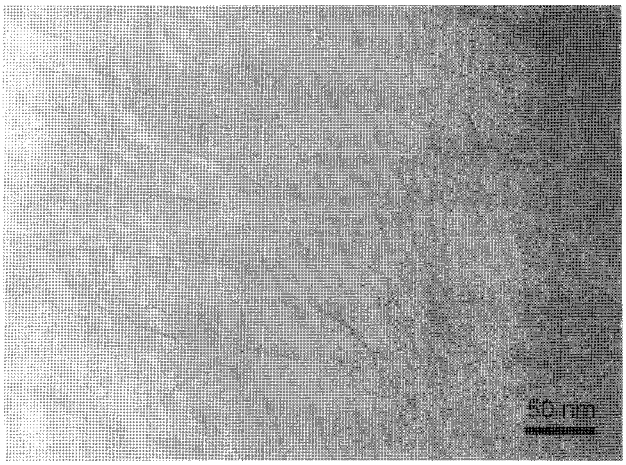

Figure 10. TEM micrograph showing that exfoliated clay layer is slightly curved shape.

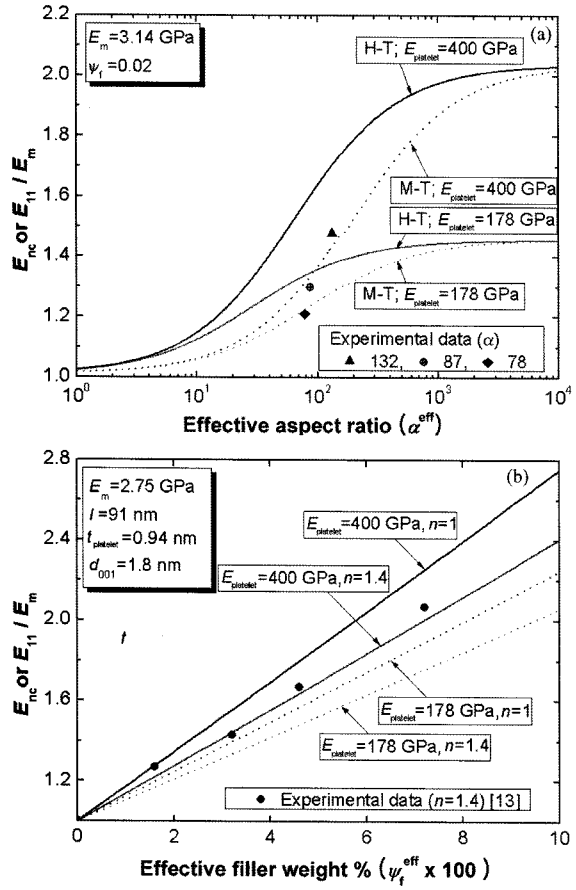

Figure 11. Comparison of experimental result and model predictions using effective filler-based model prediction; (a) completely exfoliated nanocomposites and (b) intercalated nanocomposites.

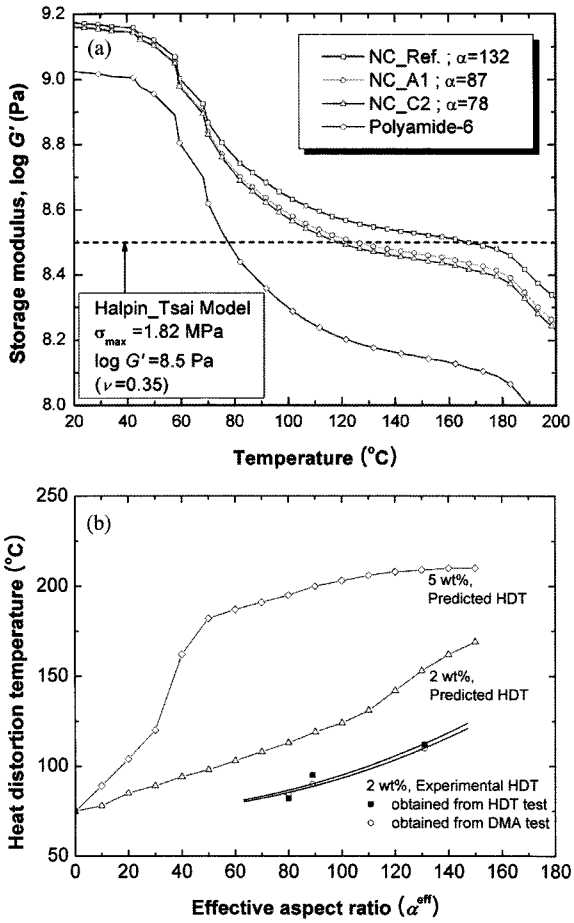

Figure 12. Model prediction of the Halpin-Tsai theory on heat distortion temperature (HDT) of nanocomposites; (a) effect of effective filler aspect ratio (α^{eff}) and (b) effect of effective filler weight fraction (ψ_f^{eff}) on HDT (experimental data included).

polymer matrix when especially considering its processing difficulties and efforts. Instead, the optimal condition regarding modulus enhancement could be determined by compromising effective filler structural parameters (n, d_{001} and S) *via* numerical simulation.

Application of Effective Filler-based Model.

Case Study I: Completely Exfoliated Nanocomposites: Experimental nanocomposite/matrix stiffness ratio (E_{nc}/E_m) is plotted as a function of effective filler aspect ratio (α^{eff}) and effective filler modulus (E_f^{eff}) at an effective fixed weight % (ψ_f^{eff} ×100) in Figure 11(a). Experimental moduli of polyamide-6/clay nanocomposites having an aspect ratio of 78, 87 and 132 are compared with those of model predictions from the Halpin-Tsai and Mori-Tanaka models. Both models roughly catch up with the modulus behaviors of the nanocomposites. When a platelet modulus ($E_{platelet}$) of 400 GPa, calculated by molecular simulation,[35] is chosen the prediction by Mori-Tanaka model reveals an excellent agreement with the experimental result, while the Halpin-Tsai model slightly overestimates. Note that the data point of aspect ratio of 78 should slightly has moved to the left since the degree of orientation for the nanocomposite is higher than that of the others.

Case Study II: Intercalated Nanocomposites: Figure 11(b) compares experimental nanocomposite/matrix stiffness ratio (E_{nc}/E_m) with effective filler-based model prediction of intercalated nanocomposites. The Mori-Tanaka model is used to evaluate the reinforcement efficiency of clay-stacked nanocomposites: the stacks had effective structural parameters, i.e., d_{001} is 1.8 nm and n is 1.4.[13] The proposed model nicely captures the corresponding experimental modulus when a filler modulus of 400 is used.

Consequently, the Mori-Tanaka model provides a reasonably accurate prediction for both intercalated and exfoliated nanocomposites.

Case Study III: Heat Distortion Temperature: Model prediction of HDT for the nanocomposites is examined. The Halpin-Tsai model is employed to predict a whole DMA storage modulus $G'(T)$, as function of temperature, for the present polyamide-6/clay nanocomposite with an aspect ratio of 78, 87 and 132, respectively. The storage modulus of nanocomposite can be estimated as following equation.[13,36]

$$E'(T) = \frac{1}{f}[2ag(E'_m - E''_m) - 2ahE'_m E''_m + bgE'_m - bhE''_m] \quad (15)$$

where a, b, f, g, and h are functions of effective filler aspect ratio (α^{eff}), effective volume fraction (ϕ_f^{eff}), E'_m, and/or E''_m (note that $E_m=2G_m(1+\nu_m)$).

The predicted $G'(T)$ is plotted as function of temperature and filler aspect ratio of the nanocomposites (Figure 12(a)). The proposed model seems to overpredict rather compared to the experimental result (Table III). This overestimation may inherently be due to the inequality of curves between the nanocomposites and the neat polyamide-6 at high temperature above T_g (note that the $G'(T)$ curves was obtained based on the curve of neat polyamide-6), as well as an assumption that the alignment of fillers is unidirectional. Nevertheless, the proposed model enables to capture the whole trend of nanocomposite curve (G' *vs.* temperature). Figure 12(b) compares the experimental HDTs obtained from both HDT and DMA tests with those predicted by the model. The predicted HDT at 2 wt% increases linearly with increasing effective filler aspect ratio, which is in good agreement with experimental HDT. Interestingly, the predicted HDT at 5 wt% dramatically increases with increasing effective filler aspect ratio at relatively low aspect ratio and then approaches a constant value. This saturation of HDT at high aspect ratio is analogous to that of E_{11}/E_m (Figure 6(b)) explained by shear lag model.

Conclusions

Continuum-based micromechanical models were employed to predict the mechanical and thermal properties of polyamide-6/clay nanocomposites. The unidirectional clay orientation and higher aspect ratios can provide a significant improvement in reinforce efficiency. Predictions of the Mori-Tanaka model considering the effective filler structural parameters, the number of platelet a stack (n) and the silicate inter-layer spacing (d_{001}), are in good accordance with experimental data. This scheme may be used to predict desirable elastic properties, which can be achieved by various processing tools, of a variety of polymer/layer-structured-nanoparticle nanocomposites, e.g., zirconium-based and graphene platelet-based nanocomposite. In addition, shear lag model also appears to be effective to address the load-transfer efficiency in nanocomposites.

References

(1) J. I. Weon and H. J. Sue, *Polymer*, **46**, 6325 (2005).
(2) H. S. Jin, J. H. Chang, and J. C. Kim, *Macromol. Res.*, **16**, 503 (2008).
(3) H. J. Sue, K. T. Gam, N. Bestaoui, N. Spurr, and A. Clearfield, *Chem. Mater.*, **16**, 242 (2004).
(4) T. Y. Hwang, J. W. Lee, S. M. Lee, and G. J. Nam, *Macromol. Res.*, **17**, 121 (2009).
(5) M. Choi, B. Lim, and J. Jang, *Macromol. Res.*, **16**, 200 (2008).
(6) P. D. Shepherd, F. J. Golemba, and F. W. Maine, *Adv. Chem. Ser.*, **134**, 41 (1974).
(7) A. Okada, Y. Fukushima, M. Kawasumi, S. Inagaki, A. Usuk, S. Sugiyami, T. Kurauchi, and O. Kamigaito, US Patent 4739007 (1988).
(8) M. Kawasumi, M. Kohzaki, Y. Kojima, A. Okada, and O. Kamigaito, US Patent 4810734 (1989).
(9) A. Usuki, Y. Kojima, M. Kawasumi, A. Okada, Y. Fukushima, T. Kurauchi, and O. Kamigaito, *J. Mater. Res.*, **8**, 1179 (1993).
(10) Y. Wang, L. Zhang, C. Tang, and D. Yu, *J. Appl. Polym. Sci.*, **78**, 1878 (2000).
(11) X. Fu and S. Qutubuddin, *Polymer*, **42**, 807 (2001).
(12) G. M. Kim, D. H. Lee, B. Hoffmann, J. Kressler, and G. Stöppelmann, *Polymer*, **42**, 1095 (2000).
(13) T. D. Fornes and D. R. Paul, *Polymer*, **44**, 4993 (2003).
(14) N. Sheng, M. C. Boyce, D. M. Parks, G. C. Rutledge, J. I. Abes, and R. E. Cohen, *Polymer*, **45**, 487 (2004).
(15) J. I. Weon, T. S. Creasy, A. J. Hsieh, and H. J. Sue, *Polym. Eng. Sci.*, **45**, 314 (2005).
(16) T. S. Creasy and Y. S. Kang, *J. Thermo. Comp. Mat.*, **17**, 205 (2004).
(17) J. I. Weon, Z. Y. Xia, and H. J. Sue, *J. Polym. Sci. Part B: Polym. Phys.*, **43**, 3555 (2005).
(18) T. D. Fornes, P. J. Yoon, H. Keskkula, and D. R. Paul, *Polymer*, **42**, 9929 (2001).
(19) J. D. Eshelby, *Proc. R. Soc. A*, **241**, 376 (1957).
(20) T. Mori and K. Tanaka, *Acta. Metall. Mater.*, **21**, 571 (1973).
(21) J. E. Ashton, J. C. Halpin, and P. H. Petit, *Primer on Composite Materials: Analysis*, Technomic, Westport, 1969.
(22) J. C. Halpin, *J. Compos. Mater.*, **3**, 732 (1969).
(23) J. C. Halpin and J. L. Kardos, *Polym. Eng. Sci.*, **16**, 344 (1976).
(24) D. Adams and D. Doner, *J. Compos. Mater.*, **1**, 152 (1967).
(25) R. Hill, *J. Mech. Phys. Solids*, **13**, 213 (1965).
(26) G. P. Tandon and G. J. Weng, *Polym. Compos.*, **5**, 327 (1984).
(27) R. Hill, *Proc. Phys. Soc. A*, **65**, 349 (1952).
(28) C. L. Tucker and E. Liang, *Compos. Sci. Technol.*, **59**, 655 (1999).
(29) H. L. Cox, *Br. J. Appl. Phys.*, **3**, 72 (1952).
(30) M. van Es, F. Xiqiao, J. van Turnhout, and van der Giessen E, *Specialty Polymer Additives: Principles and Applications*, S. Al-Malaika and A. W. Golovoy, Eds., Blackwell Science, CA Malden, MA, 2001, chapter 21.
(31) D. Hull and T. W. Clyne, *An Introduction to Composite Materials*, 2nd ed., Cambridge University Press, New York, 1996.
(32) S. Xie, S. Zhang, F. Wang, H. Liu, and M. Yang, *Polym. Eng. Sci.*, **45**, 1247 (2005).
(33) D. R. Paul and C. B. Bucknall, *Polymer Blends*, Wiley, New York, 2000.
(34) T. J. Pinnavaia and G. W. Beall, *Polymer-Clay Nanocomposites*, Wiley, New York, 2000.
(35) O. L. Manevitch and G. C. Rutledge, *J. Phys. Chem. B*, **108**, 1428 (2003).
(36) T. D. Fornes, *Polyamide-layered Silicate Nanocomposites by Melt Processing*, PhD Dissertation, University of Texas at Austin (2003).
(37) H. van Olphen, *An Introduction to Clay Colloid Chemistry, for Clay Technologists, Geologists, and Soil Scientists*, 2nd ed., Wiley, New York, 1977.